

# Group testing as a strategy for the epidemiologic monitoring of COVID-19

Vincent Brault,<sup>1,2</sup> Bastien Mallein,<sup>3,2</sup> and Jean-François Rupprecht<sup>4,2</sup>

<sup>1</sup>Université Grenoble Alpes, CNRS, Grenoble INP, LJK, 38000 Grenoble, France

<sup>2</sup>Members of the GROUPOOL collective & Participants in the MODCOV19 initiative.

<sup>3</sup>Université Sorbonne Paris Nord, LAGA, UMR 7539, F-93430, Villetaneuse, France

<sup>4</sup>Aix Marseille Univ, CNRS, Centre de Physique Théorique,  
Turing Center for Living Systems, Marseille, France

(Dated: August 30, 2022)

We propose applications of sample pooling for RT-qPCR diagnostic to the epidemiologic study of COVID-19. Taking into account the false negatives created by the dilution of individual samples, our arguments indicate that group testing allows for precise estimates of the prevalence of the disease in the population and early detection of epidemic outbreak in connected communities while saving tests for further massive testing of the population.

Regularly monitoring the *prevalence* of the contamination, i.e. the proportion of contagious individuals within the general population at a given time, is a key element to prevent the onset of an epidemic wave, to estimate the effect of social distancing policies and to anticipate a potential increase in the demand for intensive care units hospitalization [1].

Contagious individuals are generally assumed to bear a viral load in their respiratory tract [2]. Such viral load can be detected within swab samples using a technique called *reverse transcription quantitative polymerase chain reaction* (RT-qPCR) [3]. With tests performed in priority on symptomatic patients, the measured prevalence among the tested population is larger than the global prevalence, i.e. defined among the whole population. In principle, a modelling approach could provide estimates for the global prevalence in contagious viral carriers based on the statistics in the number of symptomatic individuals; however, such modeling is particularly challenging in the context of the COVID19 epidemics, given (a) the current large uncertainty regarding the proportion of asymptomatic carriers (estimated to be in 20–50% range [4–7]) and (b) the delay between the onset of contagiousity and first symptoms, which varies from 1 to 5 days [8, 9].

Testing large portions of the population, including asymptomatic individuals, would allow for a direct measure of the global prevalence. Unfortunately, the reactants of RT-qPCR diagnostic tests are a tight resource and test production would not meet the demand of such large-scale population diagnostic [10].

In such context of a global shortage in diagnostic tests, group testing has received a regain in interest. The principle of group testing consists in combining samples from multiple individuals into a single pool that is then tested using a single test-kit. The pool sample is to be positive if and only if at least one individual in the group is contaminated. The idea of group testing is not new, with a long history that dates back to 1943 [11] in the context of syphilis detection (see [12] for a review). Optimal diagnostic strategies include smart-pooling, whereby pools are organised according to lines and columns on a grid –or hypercube– with overlaps enabling the identification

of positive individuals [13–15].

Several teams across the world have achieved group testing protocols on SARS-COV2 infected individuals using RT-qPCR tests. As early as February 2020, pools of 10 have been used over 2740 patients to detect 2 positive patients over the San Francisco Bay in California [16]. A recent publication from Germany has shown that positive patients with relatively mild viral load can still be detected within pools of 30 [17]. Further works suggest that RT-qPCR viral detection can be achieved in pools ranging from 5 to 64 [18–20].

In parallel, the theoretical literature on group testing for SARS-COV-2 diagnostic is growing at a fast pace [10, 21, 22]. Most of the emphasis has been put on the binary (positive or negative) outcome of tests, with little or no regard on the viral load measure [3]. Moreover, if the possibility of false negatives is sometimes considered, it is rarely taken into account that the false negative rate increases with the dilution of samples appearing in group testing [15].

In this communication, we do not address any diagnostic problems, such as the question of determining optimal strategies to provide individual positive diagnostic to a large population using a minimal number of tests. Rather, we propose to evaluate pooling strategies for epidemiology purposes. In particular, we focus on the measure of the prevalence; we include a realistic model of RT-qPCR diagnostic tests in which we take into account the increased proportion of false negatives with larger pool sizes [25].

The rest of the article is divided into 4 parts. First, we present a simple protocol for the measurement of the prevalence in a population using group tests under the assumption of *perfect tests*, i.e. not subject to false negatives and dilution; the simplicity of this model allows us to present the main ideas behind our computations. Second, we provide a short description of the RT-qPCR test and propose a statistical model for its study. Then, we fit the parameters of this model by proposing a procedure to analyse the viral charge in patients as measured by RT-qPCR tests; our analysis is currently based on a simulated dataset that has similar statistical features as

the clinical dataset of Ref. [23]; our objective here is to provide a method to estimate the risk of false negative caused by the pooling dilution effect. Finally, we show how, using this statistical model, one can measure the viral prevalence in the population (as introduced in the first section) and design protocols to prevent an epidemic outbreak to spread within closed vulnerable communities (e.g. retirement homes, detention centres).

## I. MEASURING PREVALENCE WITH PERFECT TESTS

As discussed above, we investigate in this section the measurement of the prevalence of the disease in a population using a group testing strategy, under the assumption of *perfect* tests, i.e. with no risks of false negative.

We assume that we dispose of  $n$  tests and pools containing samples from  $N$  individuals. We denote by  $p$  the (unknown) proportion of contaminated individuals in the population. Write  $(X_i^{(N)}, i \leq n)$  the results of these tests, with  $X_i^{(N)} = 1$  if the  $i$ th test is positive, 0 otherwise. Then, these are independent and identically distributed (i.i.d.) Bernoulli random variables with parameter  $1 - (1 - p)^N$ .

**Lemma I.1.** *Writing  $\bar{X}_n^{(N)} = \frac{1}{n} \sum_{j=1}^n X_j^{(N)}$ , the quantity  $1 - (1 - \bar{X}_n^{(N)})^{1/N}$  is a strongly consistent and asymptotically normal estimator of  $p$ . A confidence interval of asymptotic level  $1 - \alpha$  is*

$$\text{CI}_{1-\alpha}(p) = \left[ 1 - (1 - \bar{X}_n^{(N)})^{1/N} \pm \frac{q_\alpha (1 - \bar{X}_n^{(N)})^{1/N-1} \sqrt{\bar{X}_n^{(N)} (1 - \bar{X}_n^{(N)})}}{\sqrt{n}N} \right], \quad (1)$$

where  $q_\alpha$  is the quantile of order  $1 - \alpha/2$  of the standard Gaussian random variable.

*Proof.* Note that  $(X_j^{(N)}, j \leq n)$  is a standard Bernoulli model, hence  $\bar{X}_n^{(N)}$  is a consistent and asymptotically normal estimator of  $f(p) = 1 - (1 - p)^N$ . Hence, using that  $f^{-1}$  is  $\mathcal{C}^1$  and Slutsky's lemma, we deduce all the above properties of the estimator  $f^{-1}(\bar{X}_n^{(N)})$  of  $p$ .  $\square$

**Remark I.2.** In particular, observe that for any  $N \in \mathbb{N}$ , the width of the confidence interval has for almost sure equivalent

$$\frac{2q_\alpha}{\sqrt{n}} \frac{(1 - p)}{N} \sqrt{\frac{1 - (1 - p)^N}{(1 - p)^N}}. \quad (2)$$

We plot in Fig. 1, for some small values of  $p$ , the total number of tests  $n$  needed so that the above quantity goes below a fixed value, as a function of  $N$ . We also plot  $nN$  the total number of tests needed in these settings.

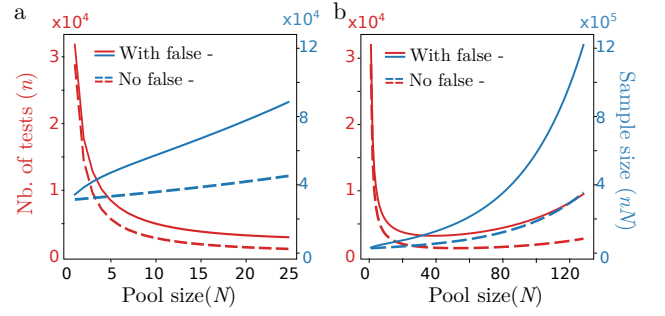


Figure 1: (a,b) Total number of tests and total number of sampled individuals in order to precisely estimate a theoretical prevalence at  $p = 3\%$  with a  $\pm 0.2\%$  precision at a 95% confidence interval as a function of the pool size  $N$  for (dashed lines) the perfect case (with no false negative) considered in Sec. I and (solid lines) the more realistic case considered in Sec. IV (with false positive; parameters are defined in Table II). In (a)  $N$  ranges from 0 to 25; in (b)  $N$  ranges from 0 to 128; as visible in (b), the plateau around the optimal pool size  $N_{\text{opt}} \approx 50$  is large: near optimal savings in tests are achieved even for moderately large pool sizes, e.g.  $N = 10$ .

A classical calculation shows that Eq. (2) is minimal for an optimal value of the individuals in the pool:

$$N_{\text{opt}} = -\frac{c_\star}{\log(1 - p)} \iff (1 - p)^{N_{\text{opt}}} \approx 0.20, \quad (3)$$

where  $c_\star = 2 + W(-2e^{-2}) \approx 1.59$  and  $W$  is the Lambert  $W$  function [10]. For  $N = N_{\text{opt}}$ , obtaining the target width takes significantly less testing than assuming single testing of individuals at random, but the total number of individuals needed to be tested is rather high, and if testing has a cost, so is sampling individuals. On the other hands, the well of the function graphed in Fig. 1 is rather wide, so a wide number of quasi-optimal choices for  $N$  can be taken with similar precision.

## II. STATISTICAL MODELLING OF THE PCR

The RT-qPCR technique has been extensively used to estimate the concentration in viral material in samples [24]. We briefly sketch the main steps of a RT-qPCR diagnostic protocol in Box 1. The PCR typically returns a  $C_t$  value, which corresponds to  $-\log_2$  of the initial number of DNA copies in the sample, up to an additive constant and measure error. It is measured as an estimated number of cycles needed for the intensity to reach a value that is larger than a target value (see Fig. 2).

PCR tests are prone to non-specific DNA amplification sequence [24, 25], which can make negative samples (whereby there viral contamination is absent) showing up positive after a certain number of cycles; such false positive typically occur after a critical number of cycles which we denoted  $d_{\text{cens}}$  (detection threshold), with is usually in the 37 to 40 range. We refer to these false positive outcomes within negative samples (whereby the virus should

### Box 1: Description of PCR tests

We review some of the steps implemented during a RT-qPCR diagnostic procedure:

1. The patient sample is treated; if present, a target viral RNA sequence is transcribed into DNA (reverse transcription);
2. The sample is placed in a PCR machine, which can measure the concentration of DNA of interest in the sample, which is characteristic of the virus;
3. A reactive is added which approximatively doubles the number of DNA of interest at every cycle;
4. The time series of the concentration in DNA over time is registered; by linear regression of the logarithm of the concentration over time, one deduces the viral concentration at the origin.

Combined measure of two viral RNA strands with a control of a human RNA strand are recommended in order to detect defective sampling that could induce false negatives, but also to improve precision of the measure as well as to normalize the number of virus copies by the quantity of human DNA [3]. We point out that the effect of reverse transcription could also induce a measurement error on the real viral concentration in the sample, which we do intend to model here.

be totally absent) as *artefacts* [25] that we model as if triggered by a vanishingly small artificial viral concentration, denoted  $\epsilon_1$ .

We propose to model for the number of cycle threshold value  $C_t$  as random variable, denoted  $Y$ , that depends on the sample viral load, denoted  $c$ , as

$$Y = -\log_2(c + \epsilon_1) + \epsilon_2, \quad (4)$$

where  $\epsilon_1$  is the law of the artefact, modelled as a log-normal distribution with parameters  $(\nu, \tau^2)$ ;  $\epsilon_2$  is an intrinsic measurement error on the threshold value  $C_t$  measurement, modelled as a centred Gaussian random variable with variance  $\rho^2$ . In the idealized no false positive artefact limit ( $\epsilon_1 \rightarrow 0$ ), the PCR threshold intensity of a negative patient ( $c = 0$ ) is never reached ( $Y \rightarrow \infty$ ).

Tests are considered to reliably positive when the number of amplification cycles is below  $d_{\text{cens}}$ , i.e. To avoid false positive, the threshold  $d_{\text{cens}}$  is chosen such that  $\mathbb{P}(\epsilon_1 > 2^{-d_{\text{cens}}})$ . Thus, using that as long as  $a$  and  $b$  are of different orders of magnitude, we have  $\log(a + b) \approx \log(\max(a, b))$ , we deduce that

$$Y(c) \approx \max(-\log_2(c), d_{\text{cens}}) + \epsilon_2, \quad (5)$$

which obeys the law of a Gaussian random variable with variance  $\rho^2$  and mean  $-\log_2(c)$ , censored at  $d_{\text{cens}}$ .

We now consider what happens when constructing a pooled sample of  $N$  individuals. For each  $i \leq N$ , we write  $z_i = 1$  if  $i$  is contaminated,  $z_i = 0$  otherwise, and  $C_i$  for the concentration in viral RNA of each sample. A combined sample is created from an homogeneous mixing

of the individual samples, the viral concentration then becomes  $\frac{1}{N} \sum z_i C_i$  (at least under the assumption of a reasonably high number of viral copies per sample). The result of the RT-qPCR measure of a grouped test with  $N$  individual then reads

$$Y^{(N)} = \max \left( \log_2 N - \log_2 \left( \sum_{j=1}^N z_j C_j \right), d_{\text{cens}} \right) + \epsilon_2. \quad (6)$$

where  $(z_i, i \leq N)$  are i.i.d. Bernoulli random variables whose parameter is the prevalence of the disease in that population;  $(C_i, i \leq N)$  are i.i.d. random variables corresponding to the law of the viral concentration within samples taken from random individuals among the overall population.

In order to determine the statistics of the group test cycle  $Y^{(N)}$ , we need a model for the statistics of  $C_j$ , the viral distribution of individuals in the overall population; this is the objective of the next section.

### III. STATISTICAL ANALYSIS OF THE VIRAL LOAD MEASURED IN POSITIVE SAMPLES

In this section, we estimate the distribution of the viral load in patients of SARS-COV-2, using the histogram presented in Fig. 1 in [23] built upon a large sample of 3712 positive patients. As the precise distribution of data points is unknown within each class of the histogram, we assumed that points were distributed uniformly within them.

In the SI Appendix B 1, we propose an estimation by mixing models which is biased from the censorship already explained above. We now suggest several ways to estimate the density of the  $C_t$  value measured by RT-qPCR among infected individuals.

#### A. Censored model and partially censored model

In this section, we present the model in the case of a single component censored to the left of a threshold  $d_{\text{cens}}$ . The experience is as follows:

1. We simulate  $X$  following a Gaussian law  $\mathcal{N}(\mu, \sigma)$ .
2. If  $X < d_{\text{cens}}$ , we return  $X$ ; otherwise, we simulate  $Z$  following a Bernoulli law  $\mathcal{B}(p)$  with  $p \in [0; 1[$  and if  $YZ = 1$ , we return  $X$  else we repeat the step 1.

We call this model a *partially censored Gaussian model* denoted  $\mathcal{CN}_{d_{\text{cens}}}(\mu, \sigma, p)$ . If we denote by  $f_{\mu, \sigma}$  (resp.  $F_{\mu, \sigma}$ ) the density (resp. the cumulative distribution function) of a Gaussian law  $\mathcal{N}(\mu, \sigma)$  then the density of  $X$  is defined for every  $x \in \mathbb{R}$  by:

$$f_X(x) = \frac{f_{\mu, \sigma}(x)}{p + (1 - p)F_{\mu, \sigma}(d_{\text{cens}})} \times \begin{cases} 1 & \text{if } x < d_{\text{cens}}, \\ p & \text{else.} \end{cases} \quad (7)$$

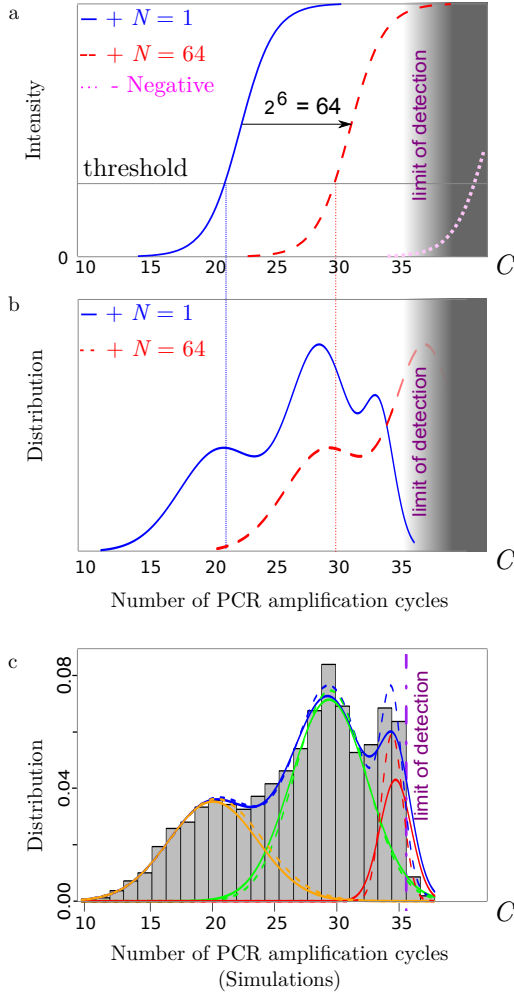


Figure 2: (a) Sketch of a RT-qPCR fluorescence intensity signal for (solid red line) a positive patient without pooling (dashed red curve) a single positive patient in a pool of 64 patients (which is expected close to that obtained by translating  $x \rightarrow x+6$  from that of a single patient) (dotted magenta curve) for a negative patient (identified as a false positive) (b) Distribution of threshold values for (solid blue line) a standard PCR, without pooling, modelled as a Gaussian mixture (see Sec. III), and (dashed red curve) within a grouped RT-qPCR tests; part of the distribution is censored beyond a limit of detection threshold value at  $Y \approx d_{\text{cens}} = 35.6$  cycles (magenta vertical line) beyond which false positive can appear. (c) Representation of the density for the censored model (fill lines) and partially censored model (dashed) with three components: the orange/green/red lines represent the density of each component and the blue line the density of the mixture. The purple vertical line corresponds to the location of the threshold  $d_{\text{cens}} \approx 35.6$ ; only the partially censored distribution uses the information in the bars to the right of this line.

*Remark III.1.* In the absence of censorship (i.e. in the limits  $p \rightarrow 1$  or  $d_{\text{cens}} \rightarrow +\infty$ ), we check that Eq. (7) converges to a Gaussian density distribution.

In this model, we assume that all values after the

threshold  $d_{\text{cens}}$  have the same probability  $p$  to appear; this can be in contradiction with the origin of the censorship exposed previously. We could imagine another law which would allow values close to  $d_{\text{cens}}$  to appear more often than those which are far away but the question would then be the choice of this law.

Another solution, which we will study here, is to *forget* the values after the threshold and to suppose that we have a *completely censored* law (ie  $p = 0$ ) which we will denote  $\mathcal{CN}_{d_{\text{cens}}}(\mu, \sigma) = \mathcal{CN}_{d_{\text{cens}}}(\mu, \sigma, 0)$  with the density defined for every  $x \in \mathbb{R}$  by:

$$f_X(x) = \frac{f_{\mu, \sigma}(x)}{F_{\mu, \sigma}(d_{\text{cens}})} \mathbb{1}_{\{x \leq d_{\text{cens}}\}} \quad (8)$$

where  $\mathbb{1}_{\{x \leq d_{\text{cens}}\}}$  is the indicator function equal to 1 if  $x \leq d_{\text{cens}}$ , and 0 otherwise.

Due to the presence of the cumulative distribution function of a Gaussian law in the denominator in the normalization constant, it is not possible to obtain analytical forms of the parameter estimators. Nevertheless, the log likelihood is regular and we can estimate the parameters using an optimization algorithm like the R function `nlm` which implements a Newton-type algorithm.

To study the quality of the estimations, we simulated  $10^4$  sample of size  $n \in \{10^2, 10^3, 10^4, 10^5\}$  following the model  $\mathcal{CN}_{d_{\text{cens}}}(0, 1, p)$  with  $d_{\text{cens}} \in \{-2, -1, 0, 1, 2, 3\}$  and  $p \in \{0, 0.1, 0.5, 0.9\}$ . We provide boxplots estimations of the parameters in Fig. S4 and a zoom on significant part in Fig. S5.

The first observation is that the estimates are generally close to the estimated value but we can sometimes have very large deviations. We find that the more  $n$  increases, the better the estimate. The threshold seems to have a weak influence on the estimation of the partially censored model but, for the fully censored model, we see that the more  $d_{\text{cens}}$  increases and the more the quality of the estimates increases; especially when  $d_{\text{cens}} = -2$  which represents approximately the 2.3% quantile. Given the large deviations that we sometimes have, it would be interesting to study if these deviations correspond to a real theoretical problem or if these hint at a need for a better optimization algorithm.

## B. Censored mixture model

Finally, we apply the previous censored models to the data simulated based on the values for the viral load distribution found in [23] with a mixture model and with a threshold  $d_{\text{cens}} \approx 35.6$  (so the last two bars are supposed to be censored.). We assume that the threshold is the same for each component. In Fig. 2(c), we represent the histogram with the density for the mixture.

We observe that densities are very close and the last component has a larger variance than that estimated by the mixture model of the section B1. To a lesser extent, the second component also extends a little further to the left of the threshold. Finally, the density of the

mixing model seems to better estimate the peaks of the histograms (the table III give the estimated parameters). For the partial censored model, the Bernoulli parameter is close to 0.2 for each component; it seems that there is a loss of 80%.

To compare the importance of the threshold, we display in Fig. S6 the censored mixture estimation with  $d_{\text{cens}} \approx 33.2$  and  $d_{\text{cens}} \approx 34.4$ . For the partial censored model, the procedure did not converge; the proportions of the bars therefore seem different and we should think about another law. So we only present for the totally censored model. We observe that the first and second components are globally unchanged. The means and standard deviations of the last component are almost the same for  $d_{\text{cens}} \approx 34.4$  and  $d_{\text{cens}} \approx 35.6$  (see table IV); only the proportions naturally decrease with the threshold. On the other hand, the mean moves slightly to the left for  $d_{\text{cens}} \approx 33.2$ ; this is due to the fact that we lose the information of the largest bars of this component. It might also be caused by our ignorance of the exact distribution of  $C_t$  values within classes of the histogram (we assume that it is an uniform distribution).

*Remark III.2.* The fact that the viral load is widely distributed further justifies the assumption leading to Eq. (5).

The current analysis is consistent with a qualitative analysis of two other datasets [19, 26], whereby we typically find that the law of  $C$  can be modelled as a log-normal distribution with a standard deviation  $\sigma$  in the 5 to 6 range.

#### IV. GROUP TESTING: APPLICATION TO EPIDEMIOLOGICAL PROBLEMS

We now show how the previous analysis of the tests used to detect COVID-19 can be used to precise the epidemiological monitoring of the disease in the general population.

##### A. Pooled sample viral concentration cannot be used to infer the precise number of infected individual

Here we show that the measured value of the pooled sample viral concentration cannot be used to estimate the number of infected individual within the pool. In the previous section, we found that the viral concentration in randomly selected infected individuals spans several order of magnitudes. Therefore, the PCR test will typically only return the concentration of the largest sample, with a drift of  $\log_2(N)$  (cf. Figure 2), using the approximation  $\log_2(\frac{1}{N} \sum a_j) \approx \log_2(\max a_j) - \log_2(N)$ . As a result, the measure from that test does not allow to detect the number of contaminated individuals in a sample, which would have been possible otherwise in the context

of a more narrower distribution (e.g. for Gaussian distributed) in the viral charge [35].

##### B. Group testing and the measure of viral prevalence

Here, in contrast to Sec. I, we no longer consider that the PCR test used to detect viral charge is perfect. Instead we used the censored group model defined in Eq. (6). With this model, it appears that increasing the value of  $N$  the size of the pool not only has the effect to increase the probability that one member of the group is contaminated, but also to decrease the smallest concentration that can be detected within samples from an infectious individual.

In these settings, we assume the prevalence in the population to be small, so that with high probability, a small number of contaminated individuals can appear in a group. Additionally, using the fact that the viral concentration is distributed on several orders of magnitudes and that the sample will return positive only if the average concentration is larger than  $d_{\text{cens}}$ , a group of  $N$  individuals will be detected as contaminated (up to a small error) if and only if at least one individual in the group has a viral charge larger than  $N2^{-d_{\text{cens}}}$ .

As we have an epidemiologic aim in mind, the apparition of additional false negatives should not be treated as disqualifying. However, this means that increasing the value of  $N$  the size of the group has the effect of decreasing the value of  $p\Phi(d_{\text{cens}}^{(N)})$ , with  $d_{\text{cens}}^{(N)} = d_{\text{cens}} - \log_2(N)$  and  $\Phi$  the cumulative distribution function of  $-\log_2(C)$  (we neglect here for simplicity the measurement error of the PCR, but the formula would work exactly the same with this additional element). Note that  $p\Phi(z_N)$  is in fact the quantity measured by the estimator described in

Table I: Table of the pool size as function of the number of tests for a prevalence of 3% measured at a  $2.10^{-3}$  precision with a 95% confidence interval, for both the perfect test (with no false negatives, see Sec. I) and imperfect tests (with false negatives; model parameters defined in Table II)

Pool size $N$	Perfect tests		Imperfect tests	
	Number of tests $n$	Sample size $nN$	Number of tests $n$	Sample size $nN$
1	29100	29100	29464	29464
2	14775	29550	15069	30138
3	10003	30009	10261	30783
5	6191	30955	6411	32055
10	3350	33500	3530	35300
20	1973	39460	2130	42600
30	1561	46830	1716	51480
50	1349	67450	1525	76250
100	1884	188400	2235	223500
200	10378	2075600	13105	2621000



### Box 2: A protocol of prevalence determination

We propose the following procedure for the measure of prevalence via group testing:

1. Start from an a priori estimate for the prevalence, denoted  $\hat{p}_0$ .
2. Based on the value of  $\hat{p}_0$ , estimate the number  $N$  of individuals in the pool that minimizes the total number of tests needed to achieve the estimation of the prevalence  $p$  at the targeted precision and confidence interval
3. Construct a number of  $n$  pools containing each  $N$  individuals selected at random in the general population.
4. Count the number of positive tests and compute the average  $\bar{X}_n^{(N)}$ .
5. An improved estimate of the prevalence then reads:  
 $\hat{p}_1 = 1 - (1 - \bar{X}_n^{(N)})^{1/N}$ .

Note that this method can easily be adapted into a Bayesian algorithm, with the number  $N$  of individuals tested modified at each iteration of the procedure.

Sec. I with the current model. As a result, the estimator of  $p$ , and its confidence interval, has to be modified into

$$\text{CI}_{1-\alpha}(p) = \left[ \frac{1 - (1 - \bar{X}_n^{(N)})^{1/N}}{\Phi(z_N)} \pm \frac{q_\alpha (1 - \bar{X}_n^{(N)})^{1/N-1} \sqrt{\bar{X}_n^{(N)} (1 - \bar{X}_n^{(N)})}}{\sqrt{n} N \Phi(z_N)} \right]. \quad (9)$$

We assume here that  $C$  is distributed according to the distribution Eq. (8) obtained in the previous section. As expected, due to false negatives we find that the number of tests needed to reach a given precision on the prevalence is increased (see Fig. 1 and Table I). We the optimal value of  $N$  to choose become smaller than  $N_{\text{opt}}$ , in particular in low prevalence settings.

Assuming a prevalence of  $p = 3\%$ , and setting up a target 95% confidence interval of width 0.4%, standard testing of individuals would require around 30 000 tests. On the other hand, taking  $N = 50$  would be optimal in the sense of Eq. (3), which would divided the needed number of tests by 20. But it would at the same time increase the number of individuals needed to be sampled by 2.5, whereas choosing  $N = 20$  already divide by 14 the number of tests needed, only increasing by 40% the size of the sample. We summarize our results in Table I.

In the current COVID19 context, we expect the overall prevalence within populations of asymptomatic individuals to be lower than 1%. Precise estimates performed in Iceland indicated a prevalence at 0.8% of the overall population [28].

We have checked that using simpler log-normal distributions for the viral load with similar mean and variance instead of Eq. (8) leads to qualitatively similar results.

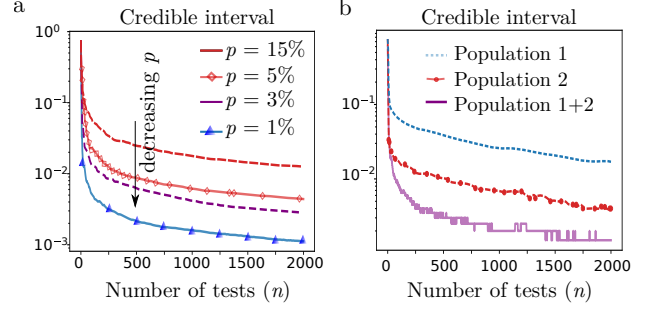


Figure 3: (a) Width of the 95% credible interval on the prevalence  $p$  with adaptative Bayesian sampling as a function of the number of tests  $n$  as compared with single pooling methods. (b) Bayesian of the credible interval in the prevalence for two-category mixed population: (magenta solid line) in the general population (blue dashed line) for the less exposed population 1 (80% of the general population with a prevalence of 0.5%); (red dotted line) for more at-risk population 2 (20% of the general population with a prevalence of 5%).

### C. Group testing and Bayesian inference of the prevalence in sub-categories of the population

Note that the above algorithm can be adapted to study different prevalences in specific sub-populations, provided that the number of individuals of each subpopulation is known for every grouped sample. In Fig. 3, we consider the problem of estimating the prevalence within two categories of the population: one at a prevalence  $p_1 = 5\%$  representing 20% of the total population, the other being at a prevalence  $p_2 = 0.5\%$ ; e.g. a prevalence of the order of 5% is typically measured among exposed health care workers [29].

*Remark IV.1.* Note that once a difference in prevalence is noted from the epidemiological study of the general population, testing can be adapted to only consider "pure" tests of these groups, and recover the total prevalence in the general population through the quotas method. The advantage of these adaptative settings is that the existence of a difference of prevalence in populations can be tested before deployment of resources needed to measure them specifically.

### D. Group testing for regular monitoring in communities

We now consider some applications of group testing to the early detection of an epidemic outbreak within a community, that is interconnected and reasonably closed to the outside (work offices, schools, retirement homes, detention centres). Our aim is to put in emphasis some properties of the screening procedures that could be put in place to detect an outbreak before it has the time to spread. We first consider the impact of using multiple

tests, and the size of the group tested to detect the existence of a contaminated individual in a group that is not contaminated. Given budget of tests to be used per unit time, we consider the effect of the regularity of tests in preventing the epidemic outbreak

### 1. Optimization of the size of pools

Here we propose a working model to solve such optimization. We consider a community of  $A$  individuals in which we assume the presence of a unique contaminated (patient 0) with a viral load  $C$  sufficiently large to be detected, i.e.  $Y < d_{\text{cens}}$ . According to the modelling in Eq. (6), the probability to detect the patient 0 in  $k$  pools of  $N$  individuals reads

$$\mathbb{P}[+|k\text{tests}] = kN\Phi(d_{\text{cens}}^{(N)})/A, \quad \text{with } kN \leq A, \quad (10)$$

where  $\Phi(d_{\text{cens}}^{(N)}) = \mathbb{P}(-\log_2(C) \leq d_{\text{cens}} - \log_2(N))$ .

We point out that, the viral load of the pre-symptomatic patient 0 may depart from Eq. (8), which is based on clinical data. For simplicity, we will consider the case of a simplified log-normal distribution  $\log N(\mu_0, \sigma_0)$ , and study the effect of a modification of the parameter  $\mu_0$ .

In Fig. 4, we represent the evolution of probability to detect the patient 0 as function of the total number of sampled individuals in a population of size  $A = 120$ . We find that there exists an optimal pool size at a value  $N = N_{\text{opt}}$  when  $\mu_0$  is close to  $d_{\text{cens}}$ , and the viral charge in patient 0 is close to being undetectable, even in small groups (top row). In this case, beyond  $N > N_{\text{opt}}$ , the risk of false negatives in large pools overcomes the potential benefit of testing larger portion of the community. However, when such high diagnostic sensibility is not needed, the detection probability becomes a monotonic function of the pool size  $N$ , indicating that larger pools are always beneficial. Moreover, if using multiple tests has an important impact on the detection probability for small  $d_{\text{cens}} - \mu_0$ , the gain is marginal as soon as the viral charge becomes large enough.

### 2. Optimization of the regularity of tests

We now consider a continuous-time steady-state version of the problem described above. We imagine that a community of  $A$  individuals is being monitored by being regularly tested every  $\tau$  units of time, and we seek the impact of this parameter  $\tau$ . Every  $\tau$  units of time,  $k$  individuals are sampled at random in the population to be tested as a pool. At a random date, which we choose to be the time  $t = 0$ , the patient 0 in the population gets contaminated, and immediately start infecting members of its community at rate  $\lambda$ . Each newly infected individual then contributes to spreading the disease at the same rate  $\lambda$ .

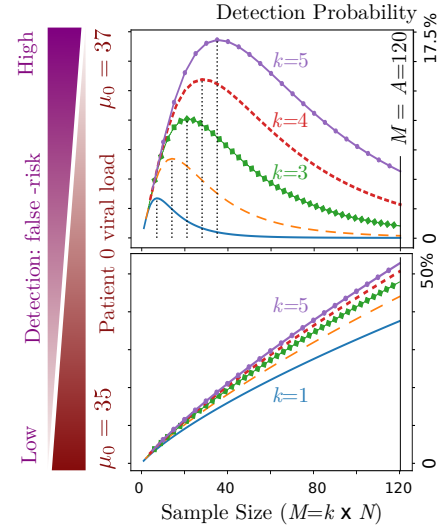


Figure 4: Early detection probability of a single patient 0 individual with low viral load  $\nu$  within a community of 120 as a function of the total sample size  $M = k \times N$ , whereby  $k$  is the total number of tests used, with (magenta solid line with circles)  $k = 5$  (dotted red line)  $k = 4$ , (green line with squares)  $k = 3$  (dashed orange line)  $k = 2$  (solid blue line)  $k = 1$ . At the onset of contagiousity, the viral charge of the patient 0 within the community is quantified in terms of a log-normal random variable  $\log N(\mu_0, \sigma_0)$  (describing the number of amplification cycles needed to detect the viral charge in a RT-qPCR machine) that is either (top) large with  $\mu_0 = 37$  modelling a patient 0 with a very low viral concentration (bottom) moderate  $\mu_0 = 30$  modelling a patient 0 with a moderate viral concentration; in both cases  $\sigma_0 = 2$ .

Table II: Table with standard parameter values. We point out that the (with std. the abbreviation of standard deviation).

Symbol	Meaning	Value
$d_{\text{cens}}$	Maximal cycle number	35.6
$\mu_i, \sigma_i, p_i$	Viral load distribution fits	Table IV
$\rho$	PCR measurement error (std.)	neglected
$\phi$	Delay before onset of symptoms	5 days
$\lambda$	External contamination rate	$0.5 \text{ days}^{-1}$
$r$	Asymptomatic probability	40 %
$\tau$	Time interval between grouped tests	1 – 10 days
$A$	Total number in the community	120 or 1000
$N$	Pool size	1–128
$\mu_0 ; \sigma_0$	Viral load of patient 0 (mean, std.)	Variable

We denote by  $r$  the proportion of asymptomatic individuals. Symptomatic individuals start showing signs of being contaminated after a given number of days after infection, denoted  $\phi$ . The outbreak is detected either if one of the screening tests finds a contaminated individual, or if symptoms appear on an individual of the community. We denote by  $T_s$  the time at which an individual in the population shows symptoms and  $T_d$  the detection time of contaminated individuals within the community.

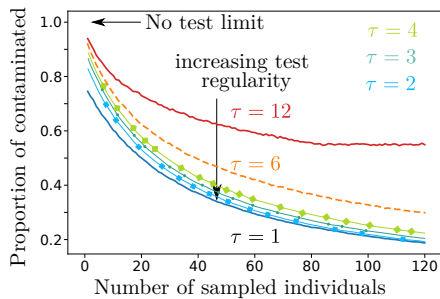


Figure 5: Proportion of contaminated individual as a function of the number of sampled individuals using  $k = 1$  tests performed at  $\tau$ -day intervals, with (solid red line)  $\tau = 12$ , (dashed orange line)  $\tau = 6$ , (dark green solid line with square)  $\tau = 4$  (light green solid line with circles)  $\tau = 3$  (cyan line with squares)  $\tau = 2$  (solid blue line)  $\tau = 1$ . Our model assumes that the entire community will eventually be contaminated if no test are performed. Here we consider a large community composed of  $A = 1000$  individuals.

In this model, the number of infected individuals at date  $t$ , denoted by  $N(t)$ , is distributed according to a geometric random variable with parameter  $1 - e^{-\lambda t}$ , as expected for such Yule process [27]. In the absence of screening tests, the average detection time is  $T_s$ , the time at which first symptoms appear, with  $\langle T_s \rangle = \phi - \log(1 - r)/\lambda$ . The average number of contaminated individuals at that time then reads:  $\langle N(T_s) \rangle = e^{\lambda \phi}/(1 - r)$ . In comparison, based on Eq. (10), we find that the first screening test after contamination will detect the outbreak with a probability

$$\mathbb{P}[+|k\text{tests}] = \frac{k(e^{\lambda \tau} - 1)(1 - q)}{\lambda \tau A}. \quad (11)$$

By the time of detection  $t = \tau$ , a number of  $\langle N(\tau) \rangle = (e^{\lambda \tau} - 1)/\lambda \tau$  individuals has been contaminated.

In Fig. 5, we compare different screening scenarios for a large community composed of  $A = 1000$  individuals (e.g. company). We vary the value of the screening time interval  $\tau$  while keeping fixed (1) the average number of tests and (2) the number of tested individuals per unit of time. Our simulation range from checks of  $k$  indi-

viduals every day to checking  $12 \times k$  individuals in 12 pools every 12 days. We compute the average number of contaminated individuals  $\langle N(T_d) \rangle$  and compare it to  $\langle N(T_s) \rangle$ . We find that screening should be made as frequent as possible. Screening for a larger subgroup always improve the outcome, but the gain in each new sampling decays after reaching around 40 individuals (see Fig. 5) representing circa 4% of the population of  $A = 1000$ .

## Conclusion

We considered the effect of sample dilution in RT-qPCR grouped tests and we proposed a model to describe the risk of false negatives as a function of the pool size. We presented a procedure to analyse experimental datasets in the viral charge of patients. Inspired by the statistical results presented in [23], we expect the statistics of the number of amplification cycles to be well described as a mixture of 3 Gaussians censored at the RT-qPCR sensibility limit. Our method could be used to distinguish at least 3 sub-populations in the individual that were tested according to their viral charge. This might be related to some medical criteria, which could be for example the severity of the symptoms as suggested in Ref. [26].

We point out that the viral load distribution that we determine here based on the clinical sampling presented in [23] is likely to be biased compared to the viral load that would be measured within the population that would be targeted in a group testing strategy, e.g. asymptomatic individuals may have a different viral load distribution than the one determined here.

We believe that group testing could provide the means for regular and massive screenings required for the early detection of asymptomatic and pre-symptomatic individuals, a particularly crucial task to succeed in the containment and potential eradication of the epidemic [8, 30, 31], as well as for the measure and study of its prevalence.

**Code accessibility** Codes will be made available upon request.

- 
- [1] H. Salje, C. Kiem, N. Lefrancq, N. Courtejoie, J. Paireau, A. Andronico, N. Hoze, J. Richet, C.-I. Dubost, H. Salje, C. Kiem, N. Lefrancq, N. Courtejoie, and P. Bosetti, (2020).
  - [2] R. Wölfel, V. M. Corman, W. Guggemos, M. Seilmaier, S. Zange, M. A. Müller, D. Niemeyer, T. C. Jones, P. Vollmar, C. Rothe, M. Hoelscher, T. Bleicker, S. Brünink, J. Schneider, R. Ehmann, K. Zwirgmaier, C. Drosten, and C. Wendtner, *Nature* (2020), 10.1038/s41586-020-2196-x.
  - [3] V. M. Corman, O. Landt, M. Kaiser, R. Molenkamp, A. Meijer, D. K. Chu, T. Bleicker, S. Brünink, J. Schneider, M. L. Schmidt, D. G. Mulders, B. L. Haagmans, B. van der Veer, S. van den Brink, L. Wijsman, G. Goderski, J.-L. Romette, J. Ellis, M. Zambon, M. Peiris, H. Goossens, C. Reusken, M. P. Koopmans, and C. Drosten, *Eurosurveillance* **25**, 1 (2020).
  - [4] K. Mizumoto, K. Kagaya, A. Zarebski, and G. Chowell, *Eurosurveillance* **25**, 1 (2020).
  - [5] Q. Bi, Y. Wu, S. Mei, C. Ye, X. Zou, Z. Zhang, X. Liu, L. Wei, S. A. Truelove, T. Zhang, W. Gao, C. Cheng, X. Tang, X. Wu, Y. Wu, B. Sun, S. Huang, Y. Sun, J. Zhang, T. Ma, J. Lessler, and T. Feng, *The Lancet Infectious Diseases* **3099**, 1 (2020).



- [6] Y. Bai, L. Yao, T. Wei, F. Tian, D.-Y. Jin, L. Chen, and M. Wang, *JAMA* **323**, 1406 (2020).
- [7] E. Lavezzo, E. Franchin, C. Ciavarella, G. Cuomo-dannenburg, L. Barzon, M. Sciro, S. Merigliano, E. Decanale, M. C. Vanuzzo, F. Onelia, M. Pacenti, S. Parisi, G. Carretta, D. Donato, K. A. M. Gaythorpe, I. College, L. C. Response, and R. Alessandra, *medRxiv*, 1 (2020).
- [8] L. Ferretti, C. Wymant, M. Kendall, L. Zhao, A. Nurtay, L. Abeler-Dörner, M. Parker, D. Bonsall, and C. Fraser, *Science* **368**, eabb6936 (2020).
- [9] N. Sethuraman, S. S. Jeremiah, and A. Ryo, *Jama* **2019**, 2019 (2020).
- [10] C. Gollier and O. Gossner, *Covid Economics*, 32 (2020).
- [11] R. Dorfman, *The Annals of Mathematical Statistics* (1943), 10.1214/aoms/1177731363.
- [12] M. Aldridge, O. Johnson, and J. Scarlett, *Foundations and Trends® in Communications and Information Theory* **15**, 196 (2019), arXiv:1902.06002.
- [13] E. Barillot, B. Lacroix, and D. Cohen, *Nucleic Acids Research* **19**, 6241 (1991).
- [14] N. Thierry-Mieg, *Nature Methods* **3**, 161 (2006).
- [15] T. Furon, [Research Report] RR-9164, Inria Rennes Bretagne Atlantique, 1 (2018).
- [16] M. Lipsitch, D. L. Swerdlow, and L. Finelli, *New England Journal of Medicine* **382**, 1194 (2020).
- [17] S. Lohse, T. Pfuhl, B. Berkó-Göttel, J. Rissland, T. Geißler, B. Gärtner, S. L. Becker, S. Schneitler, and S. Smola, *The Lancet Infectious Diseases* **3099**, 2019 (2020).
- [18] I. Torres, E. Albert, and D. Navarro, *Journal of Medical Virology*, jmv.25971 (2020).
- [19] I. Yelin, N. Aharony, E. Shaer-Tamar, A. Argoetti, E. Messer, D. Berenbaum, E. Shafran, A. Kuzli, N. Gandali, T. Hashimshony, Y. Mandel-Gutfreund, M. Halberthal, Y. Geffen, M. Szwarcwort-Cohen, and R. Kishony, *medRxiv* (2020), 10.1101/2020.03.26.20039438.
- [20] R. Ben-Ami, A. Klochendler, M. Seidel, T. Sido, O. Gurel-Gurevich, M. Yassour, E. Meshorer, G. Benedek, I. Fogel, E. Oiknine-Djian, A. Gertler, Z. Rotstein, B. Lavi, Y. Dor, D. G. Wolf, M. Salton, and Y. Drier, *medRxiv*, 2020.04.17.20069062 (2020).
- [21] A. Deckert, T. Bärnighausen, and N. Kyei, (2020), 10.2471/BLT.20.257188.
- [22] N. Sinnott-Armstrong, D. Klein, and B. Hickey, *medRxiv* (2020), 10.1101/2020.03.27.20043968.
- [23] T. C. Jones, B. Mühlemann, V. Talitha, Z. Marta, J. Hofmann, A. Stein, A. Edelmann, V. M. Corman, and C. Drosten, *Preprint Charité Hospital* (2020).
- [24] A. Forootan, R. Sjöback, J. Björkman, B. Sjögreen, L. Linz, and M. Kubista, *Biomolecular Detection and Quantification* **12**, 1 (2017).
- [25] A. Ruiz-Villalba, E. van Pelt-Verkuil, Q. D. Gunst, J. M. Ruijter, and M. J. van den Hoff, *Biomolecular Detection and Quantification* **14**, 7 (2017).
- [26] Y. Liu, L.-M. Yan, L. Wan, T.-X. Xiang, A. Le, J.-M. Liu, M. Peiris, L. L. M. Poon, and W. Zhang, *The Lancet. Infectious diseases* **2019** (2020), 10.1016/S1473-3099(20)30232-2.
- [27] S. Meleard, *Modèles aléatoires en Ecologie et Evolution*, edited by CMAP (2016).
- [28] D. F. Gudbjartsson, A. Helgason, H. Jonsson, O. T. Magnusson, P. Melsted, G. L. Norddahl, J. Saemundsdottir, A. Sigurdsson, P. Sulem, A. B. Agustsdottir, B. Eiriks-dottir, R. Fridriksdottir, E. E. Gardarsdottir, G. Georgsson, O. S. Gretarsdottir, K. R. Gudmundsson, T. R. Gunnarsdottir, A. Gylfason, H. Holm, B. O. Jensson, A. Jonasdottir, F. Jonsson, K. S. Josefsdottir, T. Kristjansson, D. N. Magnúsdottir, L. le Roux, G. Sigmundsdottir, G. Sveinbjörnsson, K. E. Sveinsdottir, M. Sveinsdottir, E. A. Thorarensen, B. Thorbjörnsson, A. Löve, G. Masson, I. Jonsdottir, A. D. Möller, T. Gudnason, K. G. Kristinnsson, U. Thorsteinsdottir, and K. Stefansson, *New England Journal of Medicine*, NEJMoa2006100 (2020).
- [29] E. S. Barrett, D. B. Horton, J. Roy, M. L. Gennaro, A. Brooks, J. Tischfield, P. Greenberg, T. Andrews, S. Jagpal, N. Reilly, M. J. Blaser, J. Carson, and R. A. Panettieri, *medRxiv*, 2020.04.20.20072470 (2020).
- [30] T. A. Treibel, C. Manisty, M. Burton, Á. McKnight, J. Lambourne, J. B. Augusto, X. Couto-Parada, T. Cutino-Moguel, M. Noursadeghi, and J. C. Moon, *The Lancet* **6736**, 19 (2020).
- [31] S. M. Kissler, C. Tedijanto, E. Goldstein, Y. H. Grad, and M. Lipsitch, *Science* **5793**, eabb5793 (2020).
- [32] R. Lebet, S. Iovleff, F. Langrognat, C. Biernacki, G. Celeux, and G. Govaert, *Journal of Statistical Software* **67** (2015), 10.18637/jss.v067.i06.
- [33] A. P. Dempster, N. M. Laird, and D. B. Rubin, *Journal of the Royal Statistical Society: Series B (Methodological)* **39**, 1 (1977).
- [34] G. Schwarz, *The Annals of Statistics* (1978), 10.1214/aos/1176344136.
- [35] We point out that the RT-qPCR measure in the viral load of samples could be used to improve efficiency and test correctness of smart pooling type diagnostic methods. We plan to investigate this aspect in future work.

## Supplementary Information

### Group testing as a strategy for the epidemiologic monitoring of COVID-19

Vincent Brault, Bastien Mallein, Jean-Francois Rupprecht

#### Appendix A: Ideal tests

We present here some of the results obtained from the computations made in Sec. I, where we assumed that we have a perfect test and used it to measure prevalence in the population. Note that with a perfect test, the question of early detection of an outbreak in a community becomes much simpler : one just need to test everyone at regular time intervals.

##### 1. Number of tests and sample size as function of the population prevalence

We trace here, for various values of the prevalence, the number of tests and total number of samples needed to archive a given precision for the confidence interval.

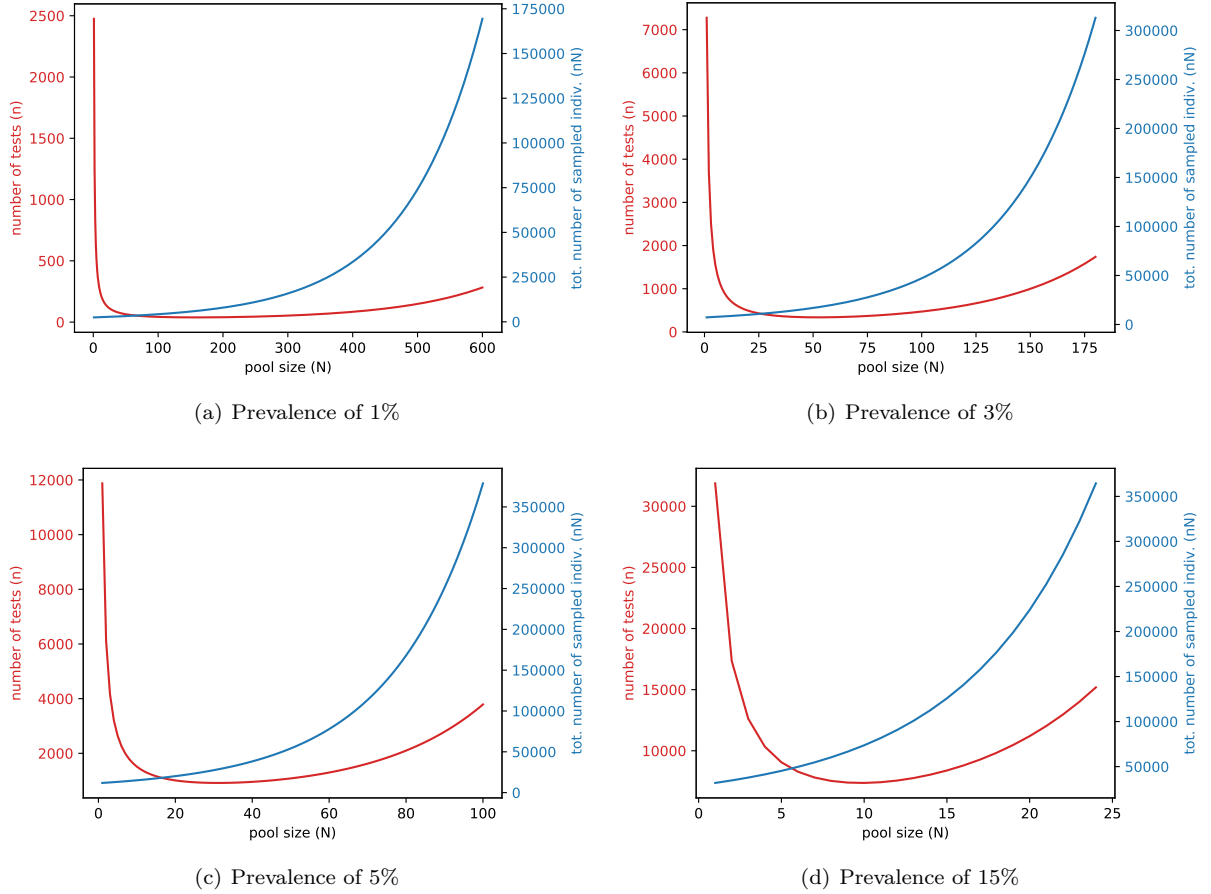


Figure S1: Total number of tests and sampled individuals so that the width of the 95% confidence interval is smaller than 0.4% as a function of the pool size  $N$  chosen for a perfect test.

## 2. Bayesian inference

We are now interested in a Bayesian approach to the measure of prevalence. We started with an initial prior distribution with density  $f_0(p) = 6p(1-p)\mathbf{1}_{\{0 \leq p \leq 1\}}$  for the prevalence, and for each new test  $j$  we do the following:

1. take the the mean value  $\bar{p}_{j-1} = \int_0^1 pf_{j-1}(p)dp$  of the prior;
2. choose the size  $N_j$  of the pool of the  $j$ th test computed as  $\left\lfloor -\frac{c_*}{\log(1-\bar{p}_{j-1})} \right\rfloor$  (cf. Eq. (3));
3. choose  $N_j$  individuals at random and test them in a group:
  - if the test is positive, then  $f_j(p) = C_j^+(1 - (1-p)^{N_j})f_{j-1}(p)$ ;
  - if the test is negative, then  $f_j(p) = C_j^-(1 - p)^{N_j}f_{j-1}(p)$ ;

with  $C_j^\pm$  normalizing constants.

We trace below the result in blue of this experiment, the 95% credible interval being  $[a_j, b_j]$ , with  $a_j$  being the 2.5%th quantile of  $f_j$  and  $b_j$  its 97.5% quantile.

We simultaneously imagine the population as being composed of two sub-populations, one large subpopulation of sparsely exposed individuals (prevalence 0.5%, representing 4/5th of the whole population), and a smaller subpopulation of very exposed individuals (prevalence 5%). Simultaneously to the previously describe experiment, we track for each test the number of individuals of each type of subpopulation that are selected (at the  $j$ th step, there are  $\text{Ber}(N_j, 0.8)$  individuals of the first subpopulation). Using this additional piece of information, we update step after step our estimation of the prevalences  $(p_1, p_2)$  in each of the two sub-populations, in the same way that we updated the law of the prevalence in the complete population.

The results are traced below in orange and green curves. One can see that the width of the credibility intervals of the sub-populations decay much slower than for the whole population. The reason is that the size of the groups are optimized to measure as precisely as possible the mean value  $p$ . However, this shows that even with group measurement, the more detailed information of the prevalence of a subpopulation of interest is not erased, and can be recovered. One could for example construct an adaptative measurement of the prevalence, in which the first half of the tests are made on the complete population, then analysed to detect sub-populations of interest, and in a second time, the second half of the tests are made on "pure" groups selected among the detected sub-populations, with group sizes chosen to identify their prevalence as precisely as possible.

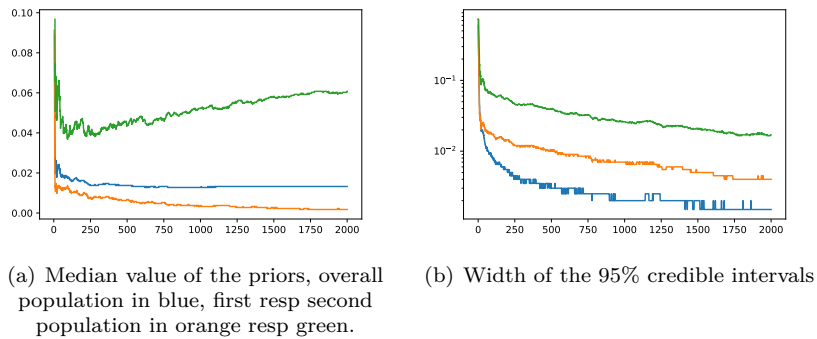


Figure S2: Bayesian estimation of the parameters of a mixed population, consisting of 80% individuals of type 1 with a prevalence of 0.5% and 20% individuals of type 2 with a prevalence of 5%.

## Appendix B: Censored Gaussians

In this section, we present the estimation based on the simple mixing models and the complementary graphs of the section III.

### 1. Naive method based on mixing models

By studying the shape of the histogram, we seem to see a mixture of three or more Gaussian distributions. To estimate the parameters, we use the R package *Rmixmod* (see [32]) using the *Expectation Maximisation* algorithm developed by [33] and we select the best model with the *Bayesian Information Criterion* (see [34]). As we simulate the data, we did the procedure 100 times in order to limit the influence of the random part. Among these 100 simulations, we obtain 95 times 3 clusters and 5 times 4 clusters. When there are 3 clusters, the estimation of the parameters is very stable (standard deviation less than 0.03 for each) but there is a little more variability in the case of 4 clusters in particular for the two classes with the largest averages (but the standard deviation does not exceed 0.25). We represent on the Fig. S3 the histogram with an example of the estimated density for each configuration.

In each configuration, we observe that the first component (in red) has a small variance. However, as recalled by [23], there is a censorship on the left which we can observe around  $s = 35.6$ : we observe that the last two classes of the histogram are very small.

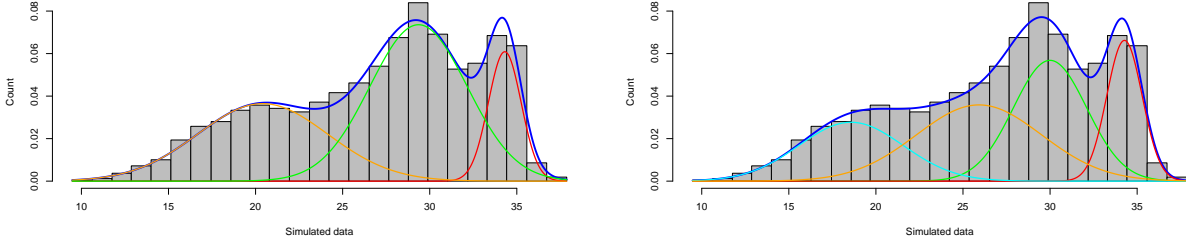


Figure S3: Representation of the histogram with the densities estimated with 3 classes (on the left) and 4 classes (on the right): the color lines (other than blue) represent the density of each component and the blue line the density of the mixture.

### 2. Censored mixture model

In this section, we present the complementary graphs of the section III.

Table III: Estimated parameters for the censored Gaussian mixture fit.

Model	$p_1$	$\mu_1$	$\sigma_1$	$\pi_1$	$p_2$	$\mu_2$	$\sigma_2$	$\pi_2$	$p_3$	$\mu_3$	$\sigma_3$	$\pi_3$
Completely		20.13	3.60	0.33		29.41	3.02	0.54		34.81	1.31	0.13
Partially	0.21	20.14	3.60	0.32	0.19	29.35	2.96	0.53	0.20	34.78	1.32	0.14

Table IV: Estimated parameters for the censored Gaussian mixture fit in function as the threshold.

$d_{\text{cens}}$	$\mu_1$	$\sigma_1$	$\pi_1$	$\mu_2$	$\sigma_2$	$\pi_2$	$\mu_3$	$\sigma_3$	$\pi_3$
35.6	20.13	3.60	0.33	29.41	3.02	0.54	34.81	1.31	0.13
34.4	20.13	3.61	0.35	29.35	2.99	0.57	34.21	1.03	0.08
33.2	19.97	3.56	0.03	29.40	3.14	0.59	33.21	1.16	0.48

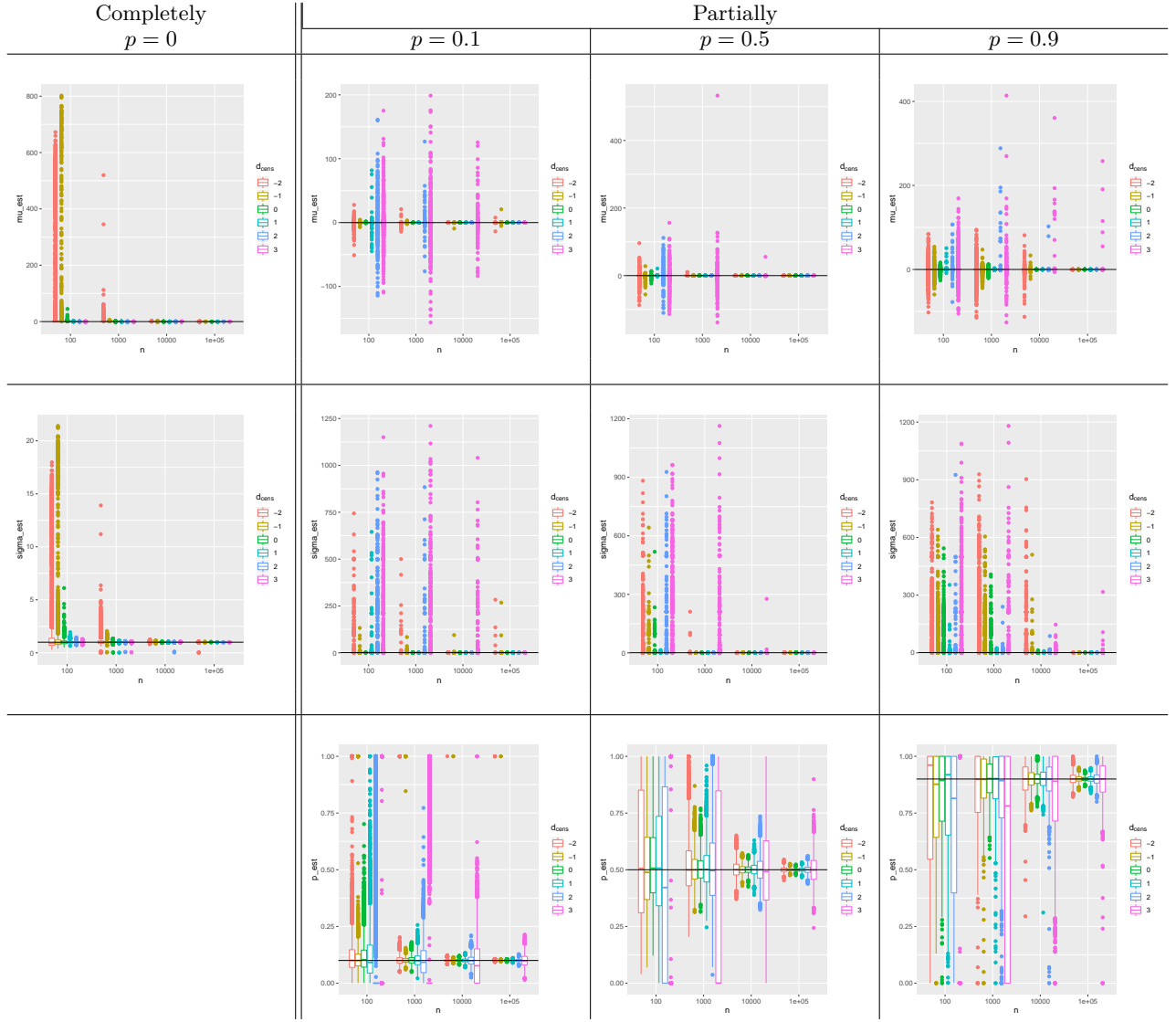


Figure S4: Boxplots of the estimations of  $\mu$  (first row),  $\sigma$  (second row) and  $p$  (last row ; only for partially censored model) in function of model (columns), the size  $n$  of sample (x-axis) and the value of the threshold  $s$  (color). The true value is symbolised by the horizontal black line.



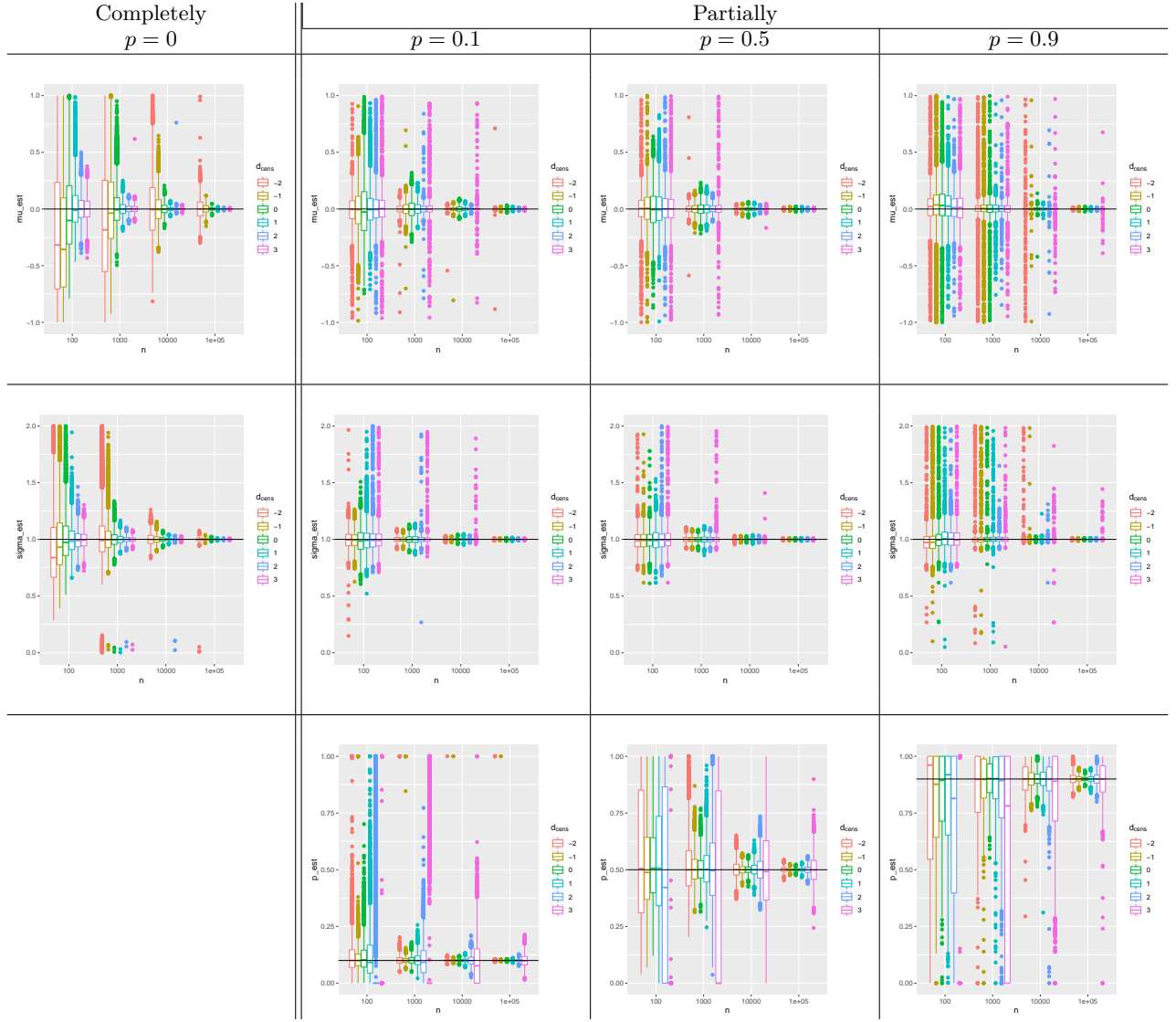


Figure S5: Zoom on boxplots of the estimations of  $\mu$  (first row),  $\sigma$  (second row) and  $p$  (last row ; only for partially censored model) in function of model (columns), the size  $n$  of sample (x-axis) and the value of the threshold  $s$  (color). The true value is symbolised by the horizontal black line.

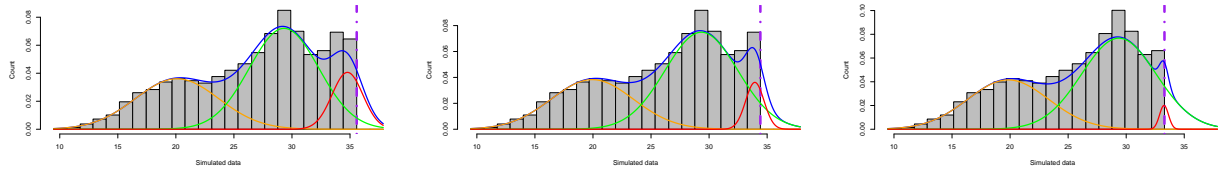


Figure S6: Representation of the density for the censored model with three components and a threshold at 35.6 (left), 34.4 (middle) and 33.2 (right): the dashed color lines represent the density of each component and the grey line the density of the mixture.